

# Supplementary materials

## Contents

Note1: Experimental setup.....	2
Control experiment .....	3
Note 2: Sample preparation .....	3
Graphene .....	3
Metal solutions .....	3
Note 3: Gold deposition .....	4
Exposure power and time dependency with 0.6 N. A. objective lens .....	4
Photon conversion efficiency .....	5
Hyperspectral Raman images .....	6
Dark field measurements of deposited gold nanoparticles.....	7
Graphing with gold .....	7
EDX spectrum of gold deposition .....	8
Note 4: Ag deposition on graphene.....	9
Deposited Ag nanoparticles on graphene .....	9
EDX spectrum of deposited Ag nanoparticles on graphene .....	10
Note 5: Deposition of Pb nanoparticles on graphene .....	10
Note 6: Deposition of Pd nanoparticles on graphene .....	11
EDX spectrum of deposited Pd nanoparticles .....	11
Graphing of Pd nano structures on graphene .....	11
Note 7: Pt deposition on graphene .....	12
Laser on-off demonstration.....	12
EDX of deposited Pt nanoparticles .....	12
Note 8: Deposition of Au/Pt mixed solution.....	13
Experimental details .....	13
Note 9: Impact of PIMD metal lines in the contact of field effect transistors .....	15

## Note1: Experimental setup

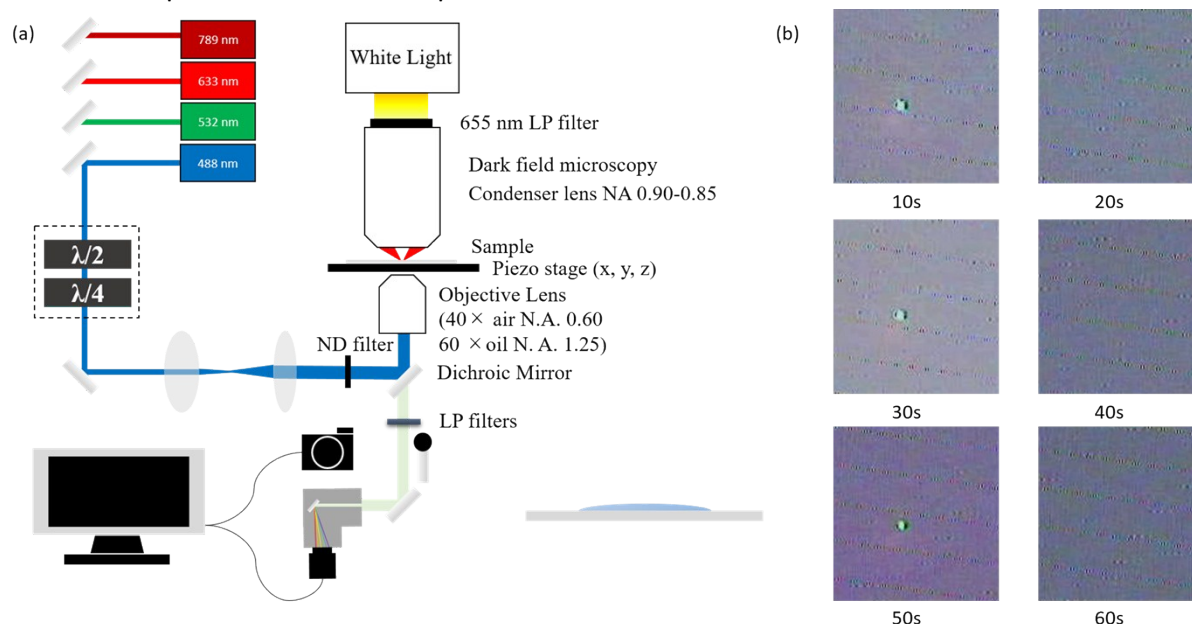


Figure S1. (a) Experimental set-up. A home-built confocal microscopy with four different lasers. The fluorescence signal is detected either by a CCD camera or a spectrometer.  $\lambda/2$ : half waveplate.  $\lambda/4$ : quarter waveplate. ND: Neutral-density. LP: Longpass. (b) Control experiment, laser excitation of the metal solution on  $\text{SiO}_2$  substrate.

Metal deposition on graphene/glass was carried out by an inverted microscope (Ti-U, Nikon), equipped with a piezoelectric stage (P517.3CL, Physik Instrument) and four different wavelength cw lasers, 785 nm (Cobolt), 633 nm (Research Electro-Optics), 532 nm (Excelsior, Spectra-Physics) and 488 nm (Stabilite 2018, Spectra-Physics), as pumping sources. Each one of the lasers beam was introduced to pass through polarizers, collimation lenses and combination of ND filters to arrange polarization state, expanding beam size and laser power, respectively. The laser on/off status was controlled by a mechanical shutter in front of the microscope. High NA objective lens (Plan Fluor,  $\times 40$ , N.A. 0.6, Nikon or Plan Fluor,  $\times 60$ , oil immersion, N.A. 1.25, Nikon) was utilized for focusing laser beam at the interface of graphene and metal ion solution. The deposition process was monitored either by wide-field optical transmission and luminescence/scattering microscopy or by confocal Raman spectroscopy. Transmission and luminescence/scattering images were recorded with a charge-coupled device (CCD) camera (ImagEM, Hamamatsu Photonics) operated at  $-30^\circ\text{C}$ , where a long pass filter (ET500lp, E550LP, HQ645LP, HQ800LP, Chroma Technology, for each pump line) was employed in front of the CCD camera to cut the elastic light scattering originating from the each laser beam. White light lamp Köhler illumination of samples was employed for the transmission imaging. The switching between transmission imaging and luminescence/scattering imaging was done by blocking the pumping laser with the mechanical shutter. Raman spectra of graphene under the same laser of 532 nm irradiation were recorded by using a CCD camera for spectroscopy (DU920P, Andor) operated at  $-30^\circ\text{C}$  coupled a polychromator (iHR320, Horiba), where a long pass filter (HQ545LP, Chroma Technology) and a pinhole (diameter  $100\ \mu\text{m}$ ) were placed before the entrance of the polychromator. A programmed movement of the piezo stage for Raman mapping was controlled using OMEGA software (AIST-NT).

Dark field (DF) spectroscopy was performed using the same microscope. A halogen lamp (12V/100W halogen lamp, Nikon) was used as the light source. Light from the lamp was focused through a DF condenser (TI-DF, dry, N.A. 0.95-0.80). Scattered light was collected by an objective lens (Plan Fluor, 40x, N.A. 0.60, Nikon) and detected with the same polychromator and CCD.

The sample was prepared by dropping metallic aqua solution on the graphene/glass.

## Control experiment

We performed the control experiment to exclude the laser induced metal deposition on SiO<sub>2</sub> directly. In the experiment, a plasma cleaned bare SiO<sub>2</sub> glass slide was mounted on the microscopy. HAuCl<sub>4</sub> solution with 1.25 mM concentration was dropped on the substrate. A 532 nm CW laser with 1.6 mW laser power was focused on the substrate. The CCD camera was used to detect the laser scattering signal when the laser was on, and white light transmission signal when the laser was blocked. It is shown in Fig. S1 (b) that after 60 s laser irradiation, no particle was formed on the substrate.

## Note 2: Sample preparation

### Graphene

Two different types of graphene samples have been used.

1. *Monolayer graphene on Si (from Graphenea Inc. [1]).*
2. *Graphene on glass cover slides.*

We used easy transfer monolayer graphene on polymer film (from Graphenea Inc. ). The following protocol was followed:

1. Released the film in the water. The graphene with sacrificial layer was detached from the substrate in the water.
2. Fished the graphene with sacrificial layers by cleaned glass slides. Transferred it on glass cover slides.
3. Put the glass cover slides on hot plate at 150°C for 1 hour.
4. Stored it in vacuum for 12 hours.
5. Removed the sacrificial layers on graphene by acetone (1 hour) and isopropanol (1 hour)

### Metal solutions

In the experiment five different types of metal solutions are prepared for metallic nano-graph on graphene.

#### *Gold nano-graphing*

We dissolved chloroauric acid trihydrate (HAuCl<sub>4</sub> · 3H<sub>2</sub>O) powder in Milli-Q water, at a concentration of 500 μM. After the light irradiation, gold nanostructures are deposited on graphene.

#### *Platinum nano-graphing*

We dissolved Chloroplatinic acid hexahydrate (H<sub>2</sub>PtCl<sub>6</sub> · 6H<sub>2</sub>O) in Milli-Q water, at a concentration of 500 μM.

#### *Silver nano-graphing*

Silver nitrate was dissolved in Milli-Q water at a concentration of 500 μM.

#### *Lead deposition*

We dissolved lead chloride ( $\text{PbCl}_2$ ) in Milli-Q water. The concentration is roughly 40 mM.

We attempt to use 1 mM at the beginning. However, no deposition has been observed.

### *Palladium nano-graphing*

Experimentally, we dissolved Palladium (II) chloride ( $\text{PdCl}_2$ ) in Milli-Q water at a concentration of 1 mM.

### Note 3: Gold deposition

Exposure power and time dependency with 0.6 N. A. objective lens

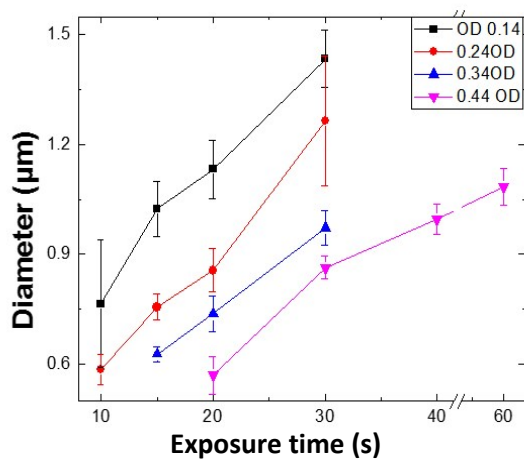
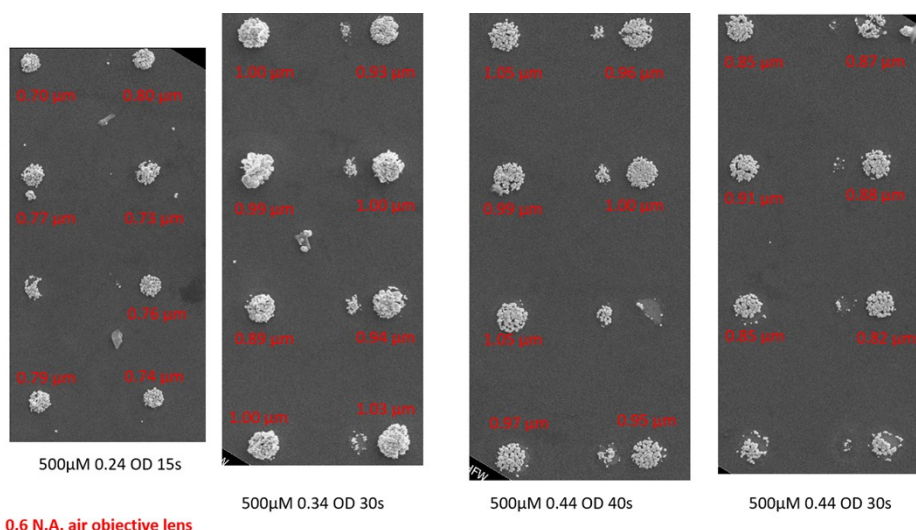


Figure S2. Impact of laser power and exposure time on the diameter of the deposited gold nanoparticles on graphene. A 0.6 N.A. air objective lens is used.

We also demonstrated the deposition of gold nanoparticles with 0.6 N.A. objective lens. The impact of exposure power and time dependency on the diameter of the gold nanoparticles is shown in Fig. S2.

The higher the laser power or the longer the exposure time is, the larger the gold nanoparticles formed.



0.6 N.A. air objective lens

Figure S3. SEM images of deposited gold nanoparticles on graphene for different exposure power or time. The  $Au^{3+}$  concentration was  $500 \mu M$ . The laser wavelength was at  $532 \text{ nm}$ . The air objective lens with  $0.6 \text{ N.A.}$  was applied.

SEM images of gold nanoparticles deposited at different laser powers and exposure times, are shown in Fig. S3. The images suggest that the deposited gold nanoparticles have uniform size distribution and good reproducibility.

#### Photon conversion efficiency

Here we describe the analysis of the impact of deposition time in more detail based on Raman spectra.

The relative deposition efficiency is obtained after correcting for the wavelength dependent Raman scattering efficiency. That scattering is basically proportional to  $\lambda^{-4}$ , where  $\lambda$  is the excitation wavelength.<sup>25</sup> Compared to the Raman scattering efficiency at  $488 \text{ nm}$ , the efficiency at  $532 \text{ nm}$  and at  $633 \text{ nm}$  is reduced by  $71\%$  and  $35\%$ , respectively. By correcting the difference in Raman scattering efficiency, the relative deposition efficiency at  $532 \text{ nm}$  and at  $633 \text{ nm}$  are calculated to be  $68\%$  and  $6\%$ , respectively. Here we have assumed that the absorbance of single layer graphene is the same for  $488 \text{ nm}$ ,  $532 \text{ nm}$ ,  $633 \text{ nm}$  and  $789 \text{ nm}$ .<sup>26</sup> The experimental results of Figure 2 (c) show that the  $785 \text{ nm}$  laser irradiation gives no deposition. The reduction potential of  $Au^{3+}$  which is  $1.69 \text{ eV}$ <sup>27</sup> corresponds to photon energy of  $733 \text{ nm}$ . When the irradiation photon energy is lower than that of  $733 \text{ nm}$  wavelength, the photo-electrons will not have enough energy to induce the reduction of gold, disfavoring particle deposition on graphene. Figure 2 (b) shows, for each wavelength, that the total amount of photons acquired for Au deposition is wavelength specific. This means that metal deposition through excited graphene is barely related to the laser power but probably to photon number. This indicates that, at the beginning, the formation process of Au nanoparticles is induced exclusively by photo-electrons and the photothermal effect is not responsible for the metal deposition.

The standard deviation in Figure 2 (b) is different for each wavelength: about  $1.3$ ,  $1.97$  and  $22.6 (\times 10^{13})$  photons, for  $488 \text{ nm}$ ,  $532 \text{ nm}$  and  $633 \text{ nm}$ , respectively. The photon energy of  $488 \text{ nm}$  is about  $2.54 \text{ eV}$  which is more than  $1.5$  times higher than the required reduction energy of  $Au^{3+}$  ( $1.69 \text{ eV}$ ). Therefore, the standard deviation of  $488 \text{ nm}$  is narrower compared to other wavelengths. Although

532 nm has lower photon energy compared to 488 nm, it is still 1.3 times higher than the necessary reaction energy, so the standard deviation is not much wider.

### Hyperspectral Raman images

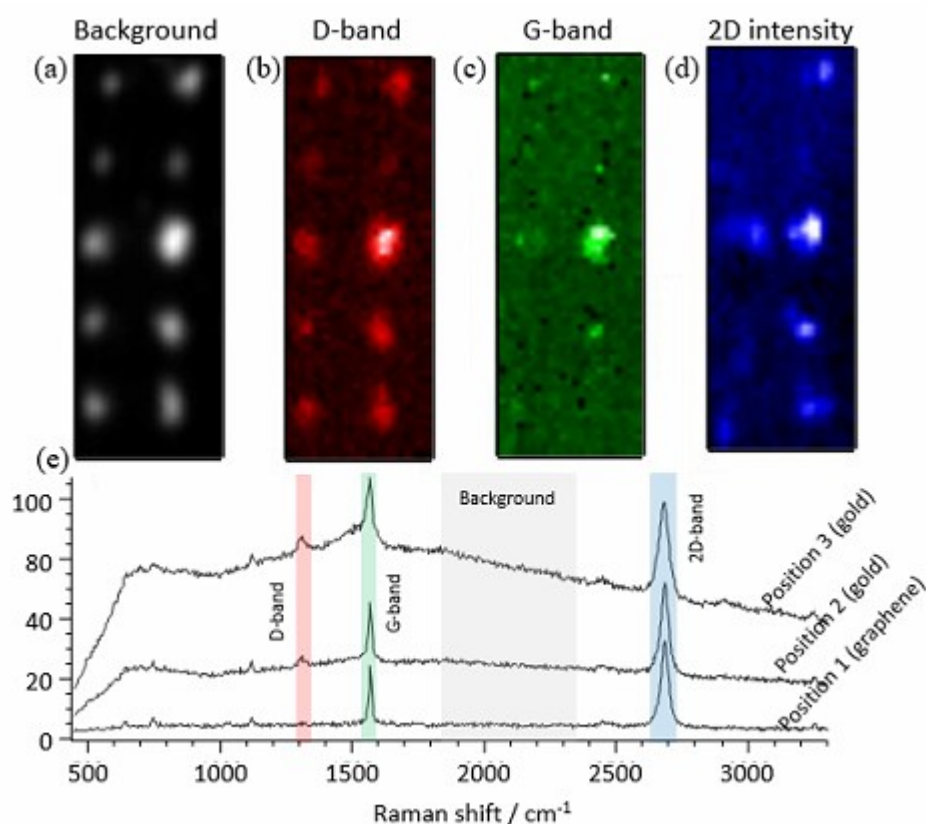


Figure S4 Raman images and spectra of individual deposited gold nanoparticles on graphene (a)-(d) The Raman images of the background, D-band, G-band, and 2D-band, respectively. (e) Temporal change of Raman spectra during deposition, where D-band, G-band and 2D-band of (a)-(d) are identified.

Here, we obtained the hyperspectral Raman images of the Au deposited graphene as shown in Figure S4. Gold scattering signals appear only on the gold deposited spots. The G-band and 2D-band present Raman enhancement due to the surface plasmon resonance. Additionally, we observed the increased intensity of graphene D-band upon deposition of Au nanoparticles. It indicates that, when Au is formed on graphene, the deposition locally changes the hybridisation of graphene from  $sp^2$  to  $sp^3$ , resulting in the appearing of graphene D-band. It was reported that the  $sp^3$  sites on graphene have higher reactivity than  $sp^2$ .

## Dark field measurements of deposited gold nanoparticles

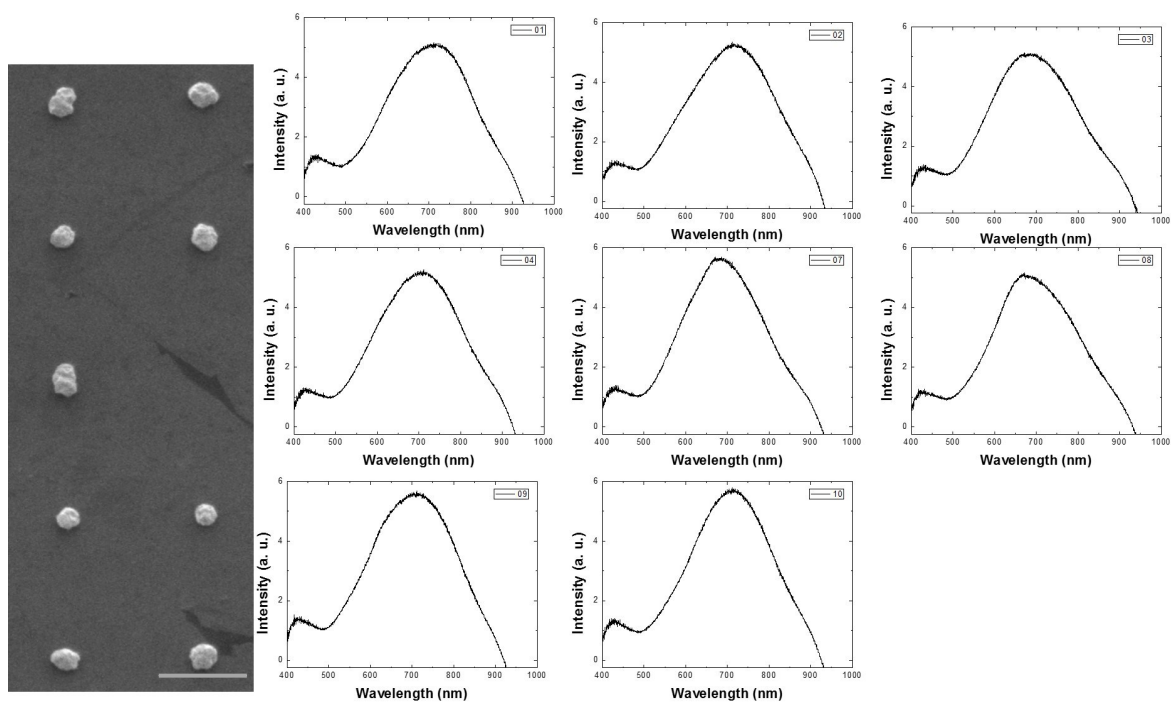


Figure S5. Left: SEM of deposited gold nanoparticles, which were deposited by a 1.25 N.A. oil objective lens. Right: Dark field spectra of individual gold nanoparticles in the left image. They present similar full width at half maximum and peak positions. The scale bar corresponds to 1  $\mu\text{m}$ .

Dark field spectrum of 8 deposited gold nanoparticles (Figure S5) The dark field spectra display a peak around 700 nm. The reproducibility indicates a good level of control of the PIMD process.

## Graphing with gold

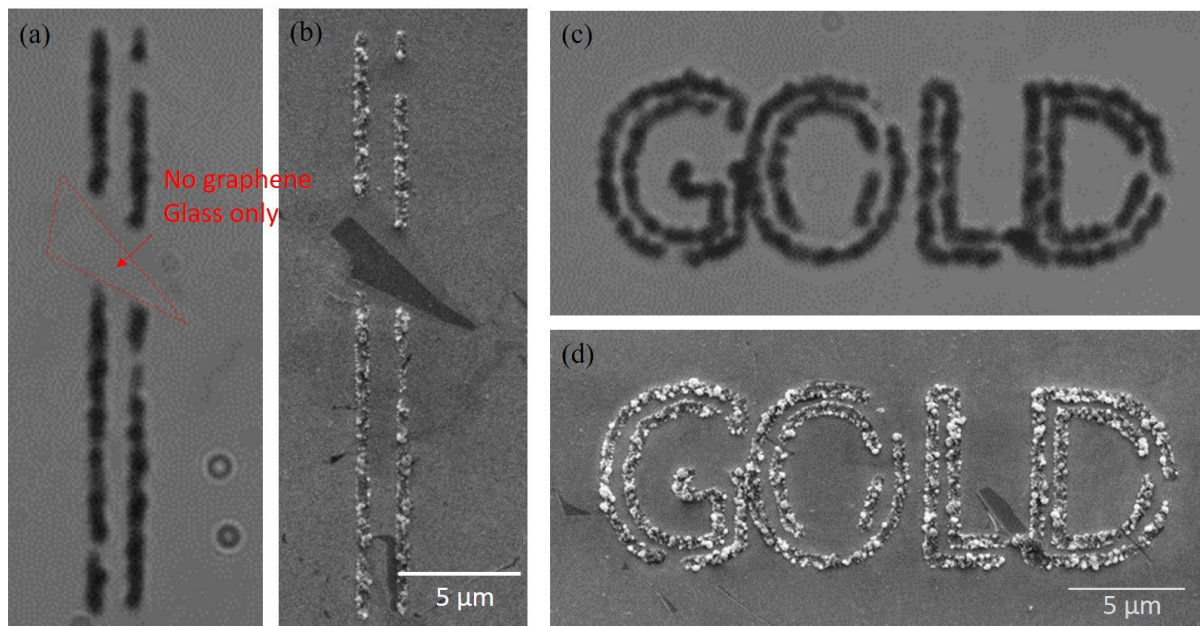


Figure S6. Gold nano-graph on graphene. (a) Wide-field microscopy image of the graphed gold nano-lines on graphene. (b) A SEM image of (a). (c) Wide-field microscopy image of graphed GOLD structure. (d) A SEM image of (c). The scale bar is 5  $\mu\text{m}$ .

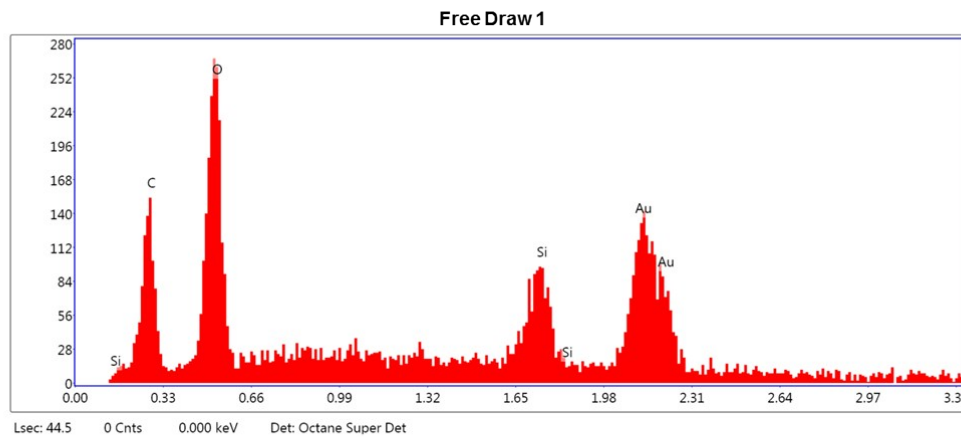
The optical microscopic image and SEM image of gold line graphing are displayed in Fig. S6 (a) and (b). The gold deposition only took place on graphene area, and not on the bare glass.

The graphed gold nanostructures are not smooth, due to strong scattering of the laser light upon their formation. Other metals, such as platinum, scatter much less under the laser irradiation conditions used, leading to a much “smoother” graphing on graphene (see Fig. 4 in main text).

EDX spectrum of gold deposition

### EDX spectrum of a deposited gold nanoparticle

kV: 5      Mag: 52372      Takeoff: 32.3      Live Time(s): 44.5      Amp Time(μs): 7.68      Resolution:(eV)129.1



### eZAF Smart Quant Results

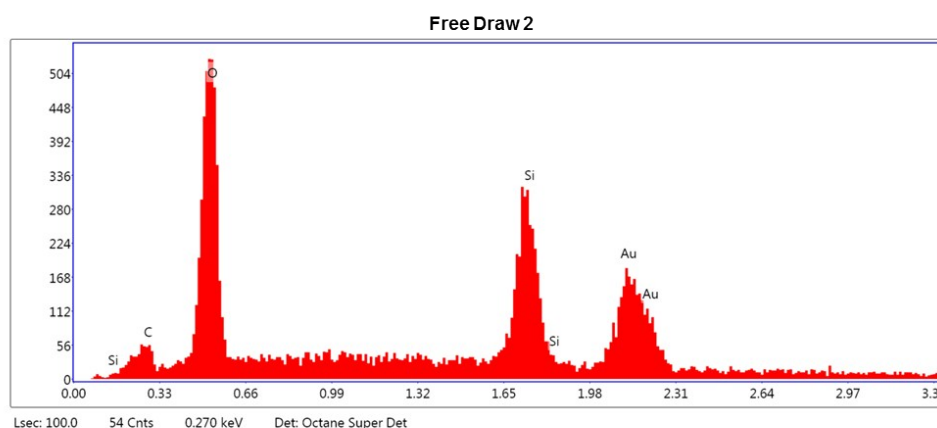
Element	Weight %	Atomic %	Net Int.	Error %	Kratio	Z	R	A	F
C K	10.21	32.89	19.19	12.64	0.0940.0942	1.6248	0.8142	0.5678	1.0000
O K	16.41	39.65	34.59	10.48	0.1660.1663	1.5290	0.8423	0.6630	1.0000
SiK	11.06	15.22	15.34	13.20	0.1430.1431	1.3598	0.9128	0.9495	1.0022
AuM	62.32	12.24	22.72	14.68	0.4630.4638	0.7066	1.1070	1.0330	1.0197

Figure S7. EDX spectrum of a deposited gold nanoparticle on graphene. C, O, Si signals originate from the graphene and SiO<sub>2</sub> substrate. Kratio, Z, R, A, F represent K ratio, atomic number correction, resolution in μm and fluorescence correction respectively. Inset graph: the SEM image of the deposited gold nanoparticle.

The energy-dispersive X-ray spectroscopy (EDX) mapping of a deposited gold nanoparticle is shown in Fig. S7. We can clearly see the Au peak. In every EDX spectrum also signals related to the presence of C, Si, and O elements appear, coming from graphene and glass cover slides.

### EDX spectrum of wide field gold deposition

kV: 5      Mag: 14591      Takeoff: 32.5      Live Time(s): 100      Amp Time(μs): 3.84      Resolution:(eV)130.6



**eZAF+ Smart Quant Results**

Element	Weight %	Atomic %	Net Int.	Error %	Kratio	Z	R	A	F
C K	3.62	10.84	4.24	16.90	0.0270.0278	1.5278	0.8410	0.5030	1.0000
O K	21.55	48.46	33.99	9.36	0.2180.2181	1.4366	0.8686	0.7046	1.0000
SiK	24.61	31.53	24.14	9.07	0.3000.3006	1.2716	0.9342	0.9586	1.0022
AuM	50.22	9.17	12.74	12.83	0.3470.3473	0.6581	1.1273	1.0294	1.0207

Figure S8. EDX spectrum of a gold structure deposited by wide-field microscopy. Inset graph: SEM image of the deposited gold structure.

We also performed the EDX spectrum on wild-field deposited gold structures. Gold signal is clearly visible in Fig. S8.

### Note 4: Ag deposition on graphene

Deposited Ag nanoparticles on graphene

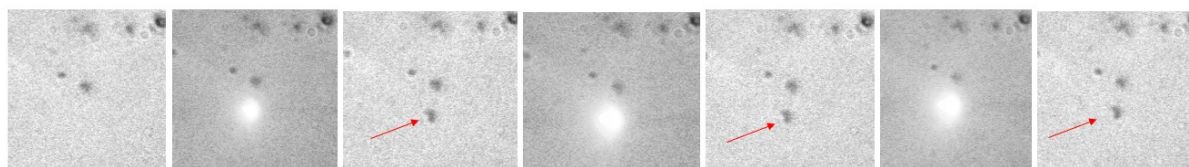


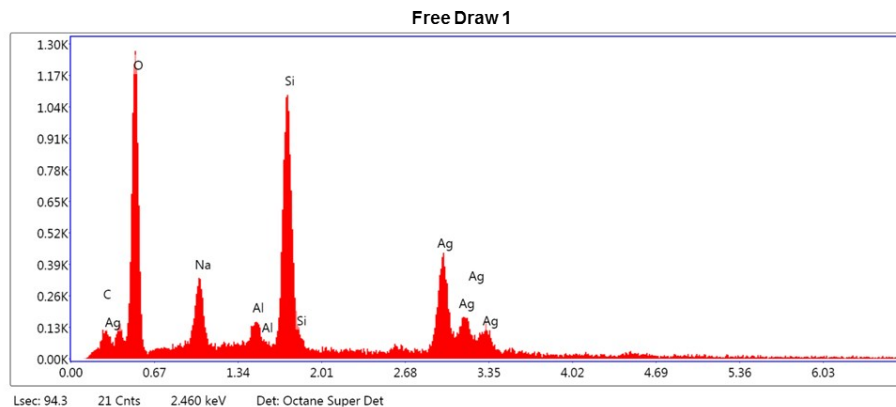
Figure S9. CCD image during the deposition of silver nanoparticles on graphene. A laser was constantly switched on and off and the transmission and scattering signal was recorded. The odd numbers of the image were taken under the transmission image conditions. The even number of the images represented the scattering signal of Ag nanoparticles under the laser illumination.

We first put the AgNO<sub>3</sub> solution on graphene, and demonstrated the Ag deposition by switching the laser on and off and meanwhile, we recorded the transmission and scattering signal from the laser irradiated spot. Fig. S9 shows that upon irradiation, a dark spot appears in the transmission images, indicating the deposition of silver nanoparticles on graphene.

EDX spectrum of deposited Ag nanoparticles on graphene

To confirm the deposited nanoparticle is silver, SEM and EDX measurements were performed. Figure S10 presents the EDX spectrum of the deposited nanoparticle. It presents clearly the silver signal, which confirms the nature of the deposited nanoparticle.

kV: 10      Mag: 17731      Takeoff: 33      Live Time(s): 94.3      Amp Time(μs): 7.68      Resolution.(eV)129.1



**eZAF Smart Quant Results**

Element	Weight %	Atomic %	Net Int.	Error %	Kratio	Z	R	A	F
C K	4.15	8.95	7.26	14.18	0.0170	1.2394	0.8964	0.3443	1.0000
O K	34.12	55.22	84.65	9.25	0.1550	1.1764	0.9208	0.3867	1.0000
NaK	6.71	7.55	22.93	9.31	0.0420	1.0589	0.9501	0.5958	1.0036
AlK	2.00	1.92	9.66	11.93	0.0160	1.0324	0.9666	0.7941	1.0116
SiK	19.97	18.42	93.66	4.93	0.1820	1.0529	0.9741	0.8583	1.0083
AgL	33.05	7.93	41.08	6.20	0.2510	0.7368	1.1475	1.0184	1.0137

Figure S10 EDX spectrum of deposited silver nanoparticles on graphene. Silver signal is clearly present. Al and Na signal is coming from the background. Inset figure: SEM image of the silver nanoparticle.

### Note 5: Deposition of Pb nanoparticles on graphene

We also deposited Pb nanoparticles on graphene. The experimental deposition conditions are similar to those of the other metals except the concentration of the ion solution. After irradiation, Pb nanoparticles are deposited on graphene as presented in main text. After we localized the Pb nanoparticles in SEM, we performed EDX measurements as plotted in Fig. S11. Upon background subtraction, weak Pb peaks appear, indicating that the deposited material is indeed Pb.

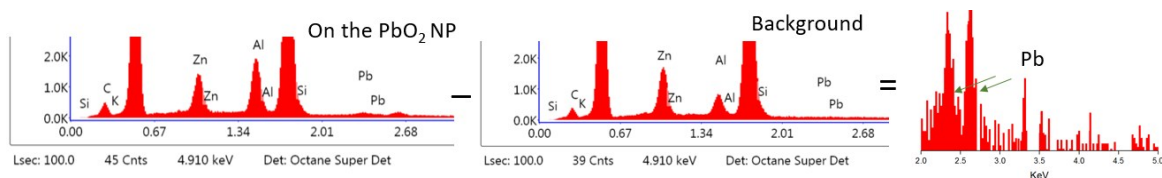
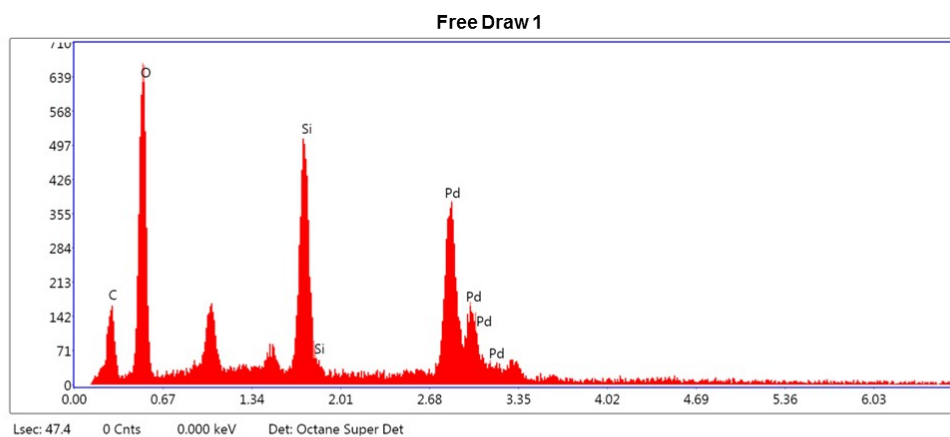


Figure S11. EDX spectrum of a deposited Pb nanoparticle on graphene.

## Note 6: Deposition of Pd nanoparticles on graphene

### EDX spectrum of deposited Pd nanoparticles

kV: 10      Mag: 21473      Takeoff: 31.9      Live Time(s): 47.4      Amp Time(μs): 7.68      Resolution:(eV)129.1



### eZAF Smart Quant Results

Element	Weight %	Atomic %	Net Int.	Error %	Kratio	Z	R	A	F
C K	4.68	11.25	12.58	13.75	0.0268	1.2905	0.8716	0.4430	1.0000
O K	33.62	60.62	90.00	10.07	0.1427	1.2261	0.8968	0.3461	1.0000
Si K	15.09	15.49	86.19	5.92	0.1440	1.1005	0.9533	0.8577	1.0113
Pd L	46.61	12.64	76.00	6.59	0.3701	0.7701	1.1267	1.0185	1.0125

Figure S12. EDX spectrum of a deposited Pd nanoparticle on graphene. The Pd peak is clearly shown. Two peaks between O and Si are coming from the background.

### Graphing of Pd nano structures on graphene

We also performed the graphing of Pd nano structures on graphene (See Fig. S13). The line quality is better than gold, however worse than Pt nano-graphing. Probably it is due to the high metal ion solution concentration (40 mM).

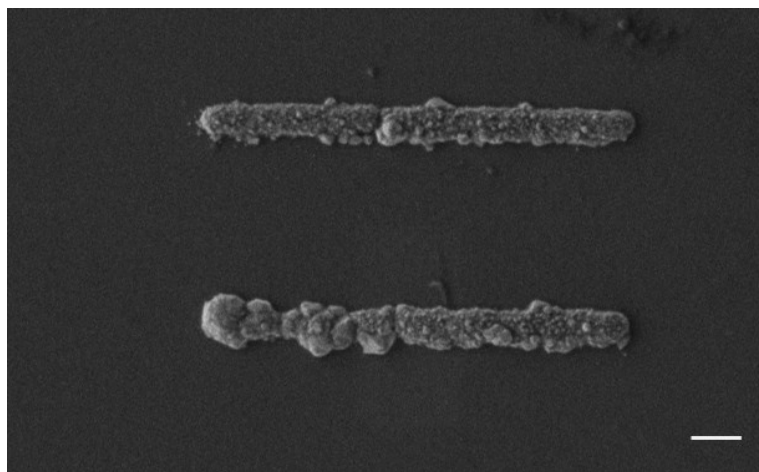


Figure S13. SEM image of the graphed Pd nano-line. The scale bar corresponds to 1 μm.

## Note 7: Pt deposition on graphene

### Laser on-off demonstration

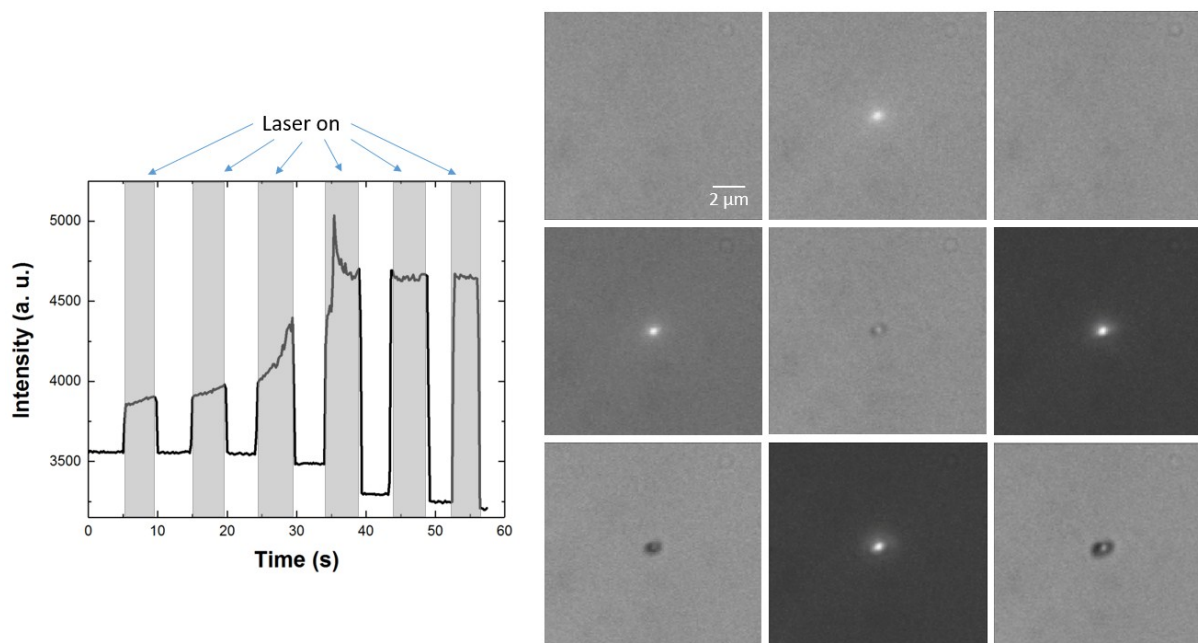


Figure S14. CCD image during the deposition of Pt nanoparticles on graphene. The laser was constantly switched on and off and meanwhile the transmission and scattering signal was recorded by the CCD camera. The longer the irradiation time, the larger the Pt nanoparticle. Meanwhile the transmission reduced during the laser irradiation.

The first deposition experiment of Pt is similar to Au deposition (Fig. 1, main text). We put  $\text{H}_2\text{PtCl}_6$  solution ( $500 \mu\text{M}$ ) on graphene, and irradiated with laser. We constantly switched the laser on and off, and meanwhile, we recorded the luminescence and the transmission when the laser is on and off (See Fig. S14). After a couple of seconds, a Pt nanoparticle is deposited on graphene. It grows larger with increasing irradiation time. We also noticed that when the Pt nanoparticle is deposited on graphene, it scatters the excitation light less than gold.

### EDX of deposited Pt nanoparticles

The EDX spectrum of the deposited Pt nanoparticle is presented in Fig. S 15, where the Pt signal is clearly visible.

kV: 5

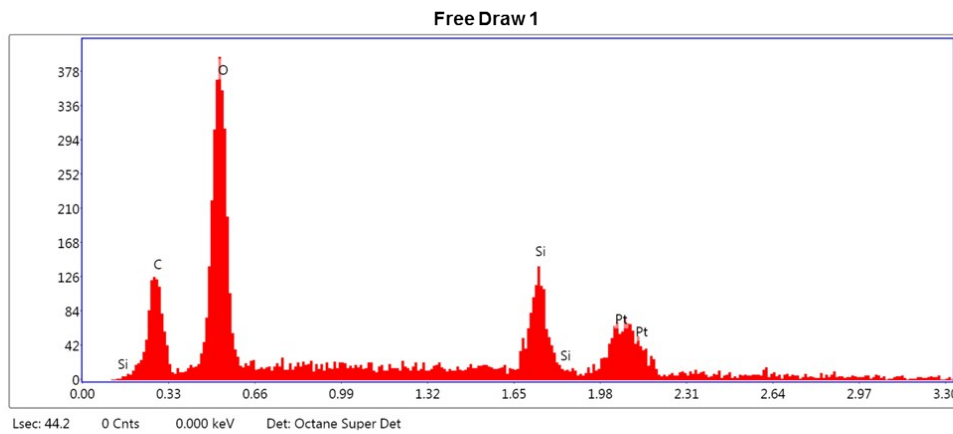
Mag: 38672

Takeoff: 32.3

Live Time(s): 44.2

Amp Time( $\mu$ s): 7.68

Resolution(eV)129.1



**eZAF Smart Quant Results**

Element	Weight %	Atomic %	Net Int.	Error %	Kratio	Z	R	A	F
C K	12.76	28.18	20.34	12.09	0.1010.1017	1.3892	0.8789	0.5738	1.0000
O K	29.85	49.51	57.40	9.15	0.2800.2809	1.3046	0.9050	0.7213	1.0000
Si K	17.93	16.94	21.00	11.13	0.1990.1994	1.1480	0.9628	0.9663	1.0023
Pt M	39.46	5.37	12.48	19.60	0.2500.2503	0.5961	1.1629	1.0432	1.0199

*Figure S15. EDX of deposited Pt nanoparticles. Pt signal is clearly resolved. The SEM image of the measured Pt nanoparticle is shown in the inset.*

## Note 8: Deposition of Au/Pt mixed solution

### Experimental details

$\text{HAuCl}_4$  and  $\text{H}_2\text{PtCl}_6$  are both mixed in water at a concentration of 500  $\mu\text{M}$  each. The solution on graphene is irradiated by a large laser beam (20  $\mu\text{m}$  diameter). After 5 min of irradiation, a big metal spot appeared. The SEM image is shown in Fig. S16, where a round spot filled with metal particles is seen.

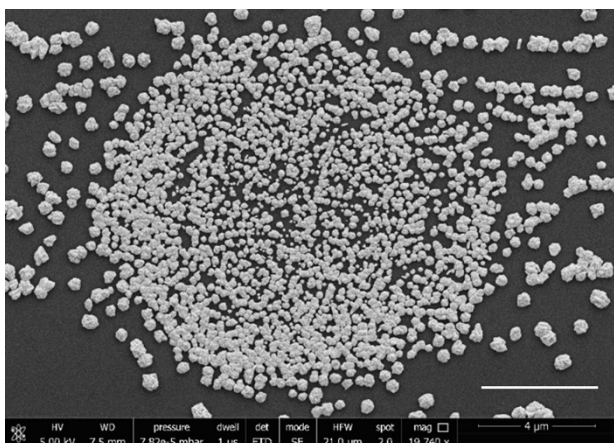
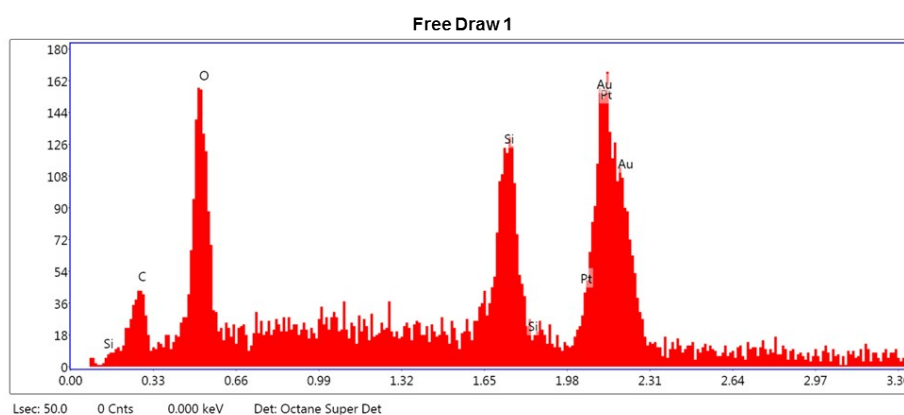


Figure S16. SEM image of deposited Pt & Au nanoparticles, created by wide-field microscopy. The scale bar represents 4  $\mu\text{m}$ .

kV: 5      Mag: 14591      Takeoff: 32.5      Live Time(s): 50      Amp Time( $\mu\text{s}$ ): 3.84      Resolution:(eV)130.6



**eZAF Smart Quant Results**

Element	Weight %	Atomic %	Net Int.	Error %	Kratio	Z	R	A	F
C K	3.99	18.44	5.91	18.30	0.0359	1.7753	0.7786	0.5065	1.0000
O K	9.40	32.61	16.80	13.69	0.0999	1.6711	0.8067	0.6360	1.0000
SiK	14.48	28.62	17.70	12.33	0.2042	1.4944	0.8828	0.9416	1.0022
PtM	0.03	0.01	0.01	99.99	0.0002	0.7847	1.0820	1.0196	1.1430
AuM	72.11	20.32	23.16	12.16	0.5849	0.7811	1.0784	1.0188	1.0193

Figure S17. EDX spectrum of the irradiated Pt & Au solution on graphene. Only the signal for Au is obtained, indicating good selectivity in this deposition process. Inset figure is the SEM image of the formed structure.

The EDX spectrum of the deposited spot (see Fig. S17) presents only gold signal. It indicates that this developed method shows high metal deposition selectivity.

### Note 9: Impact of PIMD metal lines in the contact of field effect

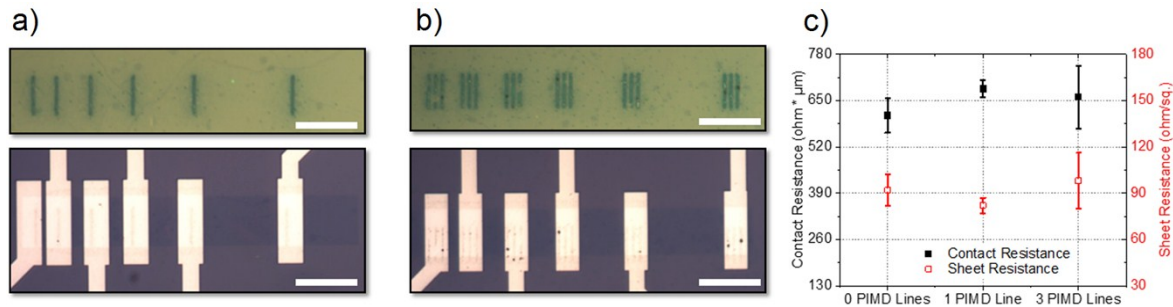


Figure S18. (a) Graphene samples with one PIMD deposited Pd line before (upper) and after (bottom) device fabrication for TLM contact resistance analysis. (b) Same as (a) for three PIMD deposited Pd lines. (c) Minimum contact resistance and sheet resistance for devices with zero, one and three PIMD deposited Pd lines below the contact ( $V_{GS} = -120V$ ). Scale bars indicate  $12 \mu m$ .

### transistors

As the PIMD deposited metal lines do not require resist or lift-off the interface with the graphene have very reduced amount of contamination. In addition, the increase in the D peak of the Raman spectra after PIMD functionalization indicate emergence of  $sp^3$  hybridization on the graphene. This gives edge-like contacts to graphene without complicate processing or patterning of the graphene before contact deposition as done in previous works.<sup>9,32,33</sup> We thus explore this possibility by extracting the resistance of devices which contacts have been enhanced by zero, one (Figure S19 (a)) or three (Figure S18 (b)) PIMD deposited Pd lines prior to metal electrode deposition. The contact resistance was extracted through the transfer length measurement (TLM) technique. For this purpose, the total resistance ( $R_T$ ) of the two probe devices with different channel length ( $L_{CH}$ ) ( $1 \mu m$ ,  $3 \mu m$ ,  $7 \mu m$  and  $18 \mu m$ ) was measured and modelled as  $R_T = 2R_c + R_{SH}(L_{CH}/W_{CH})$ . From this relation, the sheet resistance ( $R_{SH}$ ) of the graphene was obtained as a slope of the relation between  $R_T$  and  $L_{CH}$ , and the contact resistance as half of the extrapolated value of  $R_T$  toward  $L_{CH} = 0$ . The resulting extracted values for  $R_{SH}$  and the width normalized  $R_c$  are given in Figure S19 (c).

The values for both  $R_c$  and  $R_{SH}$  are marginally affected by the introduction of the PIMD lines, and the observed variations remains inside the error bars (standard deviation of measured values with respect to the fitted line). The value of the contact resistance is not reduced by increasing the amount of PIMD lines as it would have been expected from the formation of edge contacts through the PIMD lines. This can be explained by the fact that the lines are perpendicular to direction of electron flow and thus mostly only the closest line to the channel is contributing to the electron injection independently of the amount. However, the contact resistance is not degraded neither and thus demonstrates that PIMD deposition of the metal electrodes could be used as a replacement of the most conventional lift-off method used nowadays. Moreover, further experiments are required to better assess the effect of the PIMD technique on the contact interface, where the graphene is only contacted through the PIMD deposited metal and no further metal is deposited through lift-off.

## Reference

[1] D. Wei, et. al., Ultrathin rechargeable all-solid-state batteries based on monolayer graphene, *J. Mater. Chem. A*, 2013, 1, 3177.